

# Aerosol radiative effects on mesoscale cloud–precipitation variables over Northeast Asia during the MAPS-Seoul 2015 campaign

Shin-Young Park<sup>a</sup>, Hyo-Jung Lee<sup>a</sup>, Jeong-Eon Kang<sup>a</sup>, Taehyoung Lee<sup>b</sup>, Cheol-Hee Kim<sup>a,\*</sup>

<sup>a</sup> Department of Atmospheric Sciences, Pusan National University, Busan, Republic of Korea

<sup>b</sup> Department of Environmental Science, Hankuk University of Foreign Studies, Yongin, Republic of Korea

## ARTICLE INFO

### Keywords:

WRF-Chem  
Aerosol-cloud-radiation interaction  
Aerosols effects  
MAPS-Seoul 2015

## ABSTRACT

The online model, Weather Research and Forecasting Model with Chemistry (WRF-Chem) is employed to interpret the effects of aerosol-cloud-precipitation interaction on mesoscale meteorological fields over Northeast Asia during the Megacity Air Pollution Study-Seoul (MAPS-Seoul) 2015 campaign. The MAPS-Seoul campaign is a pre-campaign of the Korea–United States Air Quality (KORUS-AQ) campaign conducted over the Korean Peninsula. We validated the WRF-Chem simulations during the campaign period, and analyzed aerosol-warm cloud interactions by diagnosing both aerosol direct, indirect, and total effects. The results demonstrated that aerosol directly decreased downward shortwave radiation up to  $-44\% (-282 \text{ W m}^{-2})$  for this period and subsequently increased downward longwave radiation up to  $+15\% (\sim 52 \text{ W m}^{-2})$  in the presence of low-level clouds along the thematic area. Aerosol increased cloud fraction indirectly up to  $\sim 24\%$  with the increases of both liquid water path and the droplet number mixing ratio. Precipitation properties were altered both directly and indirectly. Direct effects simply changed cloud-precipitation quantities via simple updraft process associated with perturbed radiation and temperature, while indirect effects mainly suppressed precipitation, but sometimes increased precipitation in the higher relative humidity atmosphere or near vapor-saturated condition. The total aerosol effects caused a time lag of the precipitation rate with the delayed onset time of up to 9 h. This implies the importance of aerosol effects in improving mesoscale precipitation rate prediction in the online approach in the presence of non-linear warm cloud.

## 1. Introduction

Aerosol particles directly absorb and scatter solar and thermal infrared radiation, altering the radiative balance of the Earth's atmospheric system. This effect is referred to as the direct effect (Haywood and Boucher, 2000). Aerosol indirectly affects both cloud albedo and cloud lifetime, referred to as first and second indirect effects (Twomey, 1977; Albrecht, 1989; Pincus and Baker, 1994; Haywood and Boucher, 2000; Rosenfeld et al., 2008). The first and second indirect effects control the cloud droplet number, cloud albedo, and cloud lifetime and heights, either suppressing or enhancing precipitation. In addition to these two processes, substantially more complicated aerosol-cloud interactions have been revealed (Rosenfeld et al., 2014). As a result, a better quantification of the ever-increasing effects of aerosol-cloud-radiation interaction and its application of feedback to the daily weather prediction are also open questions, particularly in urban and polluted areas.

Northeast Asia emits large amounts of organic aerosols (OA), anthropogenic volatile organic compounds (VOCs), and particulate matter

including PM<sub>2.5</sub> and PM<sub>10</sub> (Piccot et al., 1992; Saikawa et al., 2009; Jiang et al., 2012). Specifically, the eastern regions of China, including Northeast, East, and Southeast China generate pollution composed of various emission components (Ohara et al., 2007; Li et al., 2014, 2017). Thus, characteristics associated with the development of cloud water vary depending on aerosol components and polluted regions. For example, Northeast China with temperatures below freezing is not favorable for warm cloud formation, and the North China Plain (NCP) has favorable conditions for long-lasting haze formation but not for cloud and precipitation formation, because of its relatively low amount of cloud water (Zhou et al., 2016). While East and Southeast China, with abundant cloud water, are one of the most favorable areas for cloud and precipitation formation, with increased aerosol activation and warm cloud development (Fan et al., 2012; Zhang et al., 2015). Strong air pollution characteristics over the upstream areas greatly affect downstream areas in terms of sources of emissions through the long-range transport of air masses over Northeast Asia (Carmichael et al., 2002; Park et al., 2005; Kim et al., 2012, 2017a; Wang et al., 2016). Thus, the downstream area located east of the Chinese industrial area, which

\* Corresponding author. Department of Atmospheric Sciences, Pusan National University, 2, Busandaehak-ro 63beon-gil, Geumjeong-gu, Busan, 46241, Republic of Korea.  
E-mail address: [chkim2@pusan.ac.kr](mailto:chkim2@pusan.ac.kr) (C.-H. Kim).

includes the Korean Peninsula, is expected to be significantly influenced by aerosol-cloud-radiation interactions.

To account for these aerosol effects, it is desirable to use the online-coupled meteorology-chemistry-aerosol model, which has been applied in regional meteorology and air quality simulations (Rieger et al., 2014; Tao et al., 2015; Zhou et al., 2016; Hong et al., 2017). The Weather Research and Forecasting model with Chemistry (WRF-Chem) is one such fully coupled online model (Grell et al., 2005; Peckham et al., 2011). The WRF-Chem is capable of simulating feedback between aerosols and meteorology for various atmospheric processes by linking aerosol optical properties to the radiation scheme and cloud condensation nuclei (CCN) potential to the microphysics scheme (Gustafson et al., 2007; Chapman et al., 2009). Several studies revealed that meteorological fields and air quality significantly improve model performance when aerosol feedback is considered in the WRF-Chem simulation (Chapman et al., 2009; Wang et al., 2015b; Wu et al., 2017). Previous studies using WRF-Chem for indirect effects focused on marine stratocumulus clouds with relatively clean air quality conditions, which can be resolved at coarser resolutions (Yang et al., 2011; Saide et al., 2012; Grosvenor et al., 2017). Furthermore, other studies pointed out that aerosol feedback focuses on either global or seasonal scales, and ignored shorter time scales (Gao et al., 2017; Song et al., 2017).

Previous analyses that employed satellite data also stressed the importance of aerosol-cloud-radiation interaction over Northeast Asia (Wang et al., 2014, 2015a; Kourtidis et al., 2015). For example, some studies highlight the negative relationship between cloud droplet radius and aerosol optical depth (AOD) over the East China Sea, which is in agreement with the first indirect effect known as Twomey's effect (Rosenfeld, 2000; Kim et al., 2003). Other researches (e.g., Wang et al., 2014; Kourtidis et al., 2015) exploring the relationship between AOD and cloud cover overestimate (underestimate) the AOD impact on cloud cover in regions where AOD and water vapor have similar (opposite) seasonal variations. However, these findings also have many limitations in quantitatively determining the mechanism of aerosol effect for two main reasons. The first is the inability to distinguish the contribution of aerosols to the observed cloud variation, and the second is the difficulty in obtaining region-specific observation data such as the vertical profile and absorption of aerosols.

The present modeling study was conducted as part of the Megacity Air Pollution Study-Seoul (MAPS-Seoul) 2015 campaign from 18 May 2015 to 13 June 2015 and investigated the manner in which regional aerosol-cloud-radiation interactions are captured in WRF-Chem. The study period was the MAPS-Seoul 2015 campaign, which is a pre-campaign of the Korea-United States Air Quality (KORUS-AQ) study. KORUS-AQ is an international, multi-organizational mission created to observe air quality across the Korean Peninsula and its surroundings (Lee and Kim, 2016; Kim et al., 2017b).

The objectives of this study are to evaluate the complex interactions between aerosol and meteorological fields using the coupled online WRF-Chem model over Northeast Asia, where sources of abundant aerosols create favorable conditions for developing warm cloud processes. Furthermore, this study characterizes the influences of aerosol feedback on meteorological fields during the MAPS-Seoul 2015 campaign. And we diagnose aerosol effects to improve meteorological and chemical forecasting for shorter time scales such as diurnal or weekly cycles.

## 2. Data and methodology

### 2.1. MAPS-Seoul 2015 campaign and aircraft data

During the MAPS-Seoul 2015 campaign period, seven research flights (RFs), RF1 to RF7, were carried out near the Seoul Metropolitan Area (SMA) in Korea. Our modeling domain and flight tracks are presented in Fig. S1 and the flight numbers and take-off/landing times are reported in Table S1. RF1 was test flight without spiral flight over SMA

and RF2 flew to different two heights over the Yellow Sea. RF3 and RF6 included spiral flights over the Yellow Sea to analyze the vertical structures of aerosols. RF5 travelled to the metropolitan cities of Gwangju and Busan, and returned to base (Fig. S1b). A High Resolution Time-of-Flight Aerosol Mass Spectrometer (HR-ToF-AMS, Aerodyne Research Inc., Billerica, MA, USA) and an Ultra-High Sensitivity Aerosol Spectrometer (UHSAS, Droplet Measurement Technologies Inc., Boulder, CO, USA) were installed on the Hanseo KingAir-C90GT aircraft (Textron Aviation Inc., Wichita, KS, USA). In this study, RF4 and RF7 were used to evaluate the results of WRF-Chem model, because both flights show the meteorological signal of the long-range transport process from China. RF4 and RF7 flew from Taean (base) to Seoul and Wonju, took samples below an altitude of 2500 m, and then returned along a similar track.

All seven RF excursions were equipped with the HR-ToF-AMS onboard during the campaign. The operation of the HR-ToF-AMS is based on ambient air pulled through a cyclone (URG Corporation, Chapel Hill, NC, USA) at a flow rate of  $3 \text{ L min}^{-1}$  to remove particles with aerodynamic diameters larger than  $2.5 \mu\text{m}$  in front of the HR-ToF-AMS. Ambient air enters the HR-ToF-AMS through a pressure drop critical orifice  $110 \mu\text{m}$  in diameter with an average inlet flow rate of  $0.105 \text{ L min}^{-1}$ . An aerodynamic lens focuses ambient particles of  $\sim 35 \text{ nm}$  to  $\sim 1 \mu\text{m}$  into a narrow beam to create the particle beam, which then flows into the Particle Time-of-Flight (PToF) region. Non-refractory particles, with the aerodynamic diameter of  $d < 1 \mu\text{m}$ , are vaporized on impact with a resistively heated surface at  $\sim 600^\circ\text{C}$  and ionized by electron ionization at 70 eV. The operation of the HR-ToF-AMS is described in detail elsewhere (Jayne et al., 2000; Jimenez et al., 2003; Drewnick et al., 2005; DeCarlo et al., 2006; Canagaratna et al., 2007; Lee et al., 2015).

In this study, the HR-ToF-AMS was operated under V-mode, and an MS mode of 20 s time resolution was used to determine the compositions of non-refractory particles including the concentrations of OA, nitrate, sulfate, ammonium and chloride. The HR-ToF-AMS was calibrated for ionization efficiency (IE) by using 350 nm ammonium nitrate particles at a number density of  $\sim 300 \text{ cm}^{-3}$ . The values of the relative IE for other aerosol types including OA, sulfate, nitrate, ammonium and chloride were derived from default values.

### 2.2. Other observational data used in this study

The WRF-Chem model results were compared with meteorological observations. The meteorological observation data of 91 stations located over the southern part of the Korean Peninsula were obtained from the Korea Meteorological Administration (KMA) (Fig. S1b). The Tropical Rainfall Measuring Mission (TRMM) was also employed in this study to validate the simulated precipitation results (Huffman et al., 2007). TRMM is an integral part of the National Aeronautics and Space Administration (NASA) Earth Science Enterprise, and provides satellite-derived estimates of tropical/subtropical precipitation across the globe and estimates the associated latent heating. The 3B42 product produces three-hourly merged high-quality infrared and microwave precipitation estimates at a spatial resolution of  $0.25^\circ \times 0.25^\circ$ . The spatial coverage extends from  $50^\circ\text{S}$  to  $50^\circ\text{N}$  latitude, covering our study domain over Northeast Asia.

### 2.3. Model, configuration, and data used

The employed meteorological model, WRF is a fully compressible and non-hydrostatic mesoscale numerical weather prediction model (Skamarock et al., 2008). WRF-Chem is an online-coupled meteorology-chemistry-aerosol model that can simultaneously simulate trace gases and aerosols with WRF meteorological fields. The air quality and meteorological components use the same advection scheme, grid, and physics schemes for sub-grid scale transport (Grell et al., 2005; Fast et al., 2006). Version 3.7.1 of WRF-Chem was employed in this study.

**Table S2** summarizes the model configuration.

WRF-Chem was designed to simulate aerosol-cloud-radiation interaction with existing model treatments for various feedback processes of direct and indirect aerosol effects. To calculate the direct effect, aerosol optical properties such as extinction, single scattering albedo, and the asymmetry factor for scattering were calculated as functions of wavelength and three-dimensional position. The current study employed the Rapid Radiative Transfer Model for the General Circulation Models (RRTMG) scheme to generate these radiative properties. Each aerosol chemical component has its own associated complex refractive index calculated according to the volume averaging approximation for each size mode. The Mie theory was applied to estimate extinction and scattering efficiencies. For efficient computation, the methodology described by Ghan et al. (2001) was employed. The net radiative impacts were calculated by passing the bulk optical properties of the aerosol layer to the radiative transfer parameterization. Fast et al. (2006) and Barnard et al. (2010) describe the aerosol optical property calculation in detail.

For aerosol indirect effects, aerosol-cloud interaction is a complicated process that involves activation and resuspension of aerosol particles, aqueous chemistry, and wet removal. The activation process in WRF-Chem is based on the maximum supersaturation, which is determined from a Gaussian spectrum of updraft velocities and the bulk hygroscopicity of each aerosol compound for all log-normal modes of particles (Abdul-Razzak and Ghan, 2000, 2002). Wet removal of aerosols and trace gases is treated both in and below clouds. Within clouds, aerosols and trace gases dissolved in the water are collected by precipitation such as rain, snow, and graupel. The wet scavenging module by precipitation below clouds was parameterized following the method of Easter et al. (2004). However, because of the irreversible removal process of aerosols by rain, resuspension of aerosol particles from evaporated rain is not possible in the current version of the model.

To simulate the indirect effects, the scheme of activation, resuspension, and wet scavenging for aerosol particles needs to be coupled with a double-moment microphysical scheme that predicts the number and mass concentrations for hydrometeors. The Morrison microphysics scheme used in this study includes the prognostic treatment of the cloud droplet number concentration, which considers the losses caused by collision, coalescence, collection, and evaporation, and the sources caused by nucleation. In addition, the Morrison scheme accounts for the autoconversion of cloud water to rain water depending on the cloud droplet number (Liu et al., 2005). Therefore, aerosol activation affects both the rain rate and liquid water content. The couplings were implemented for warm cloud processes only, and direct links of aerosols with ice nuclei (IN) were not considered in this study.

In this study, a 27 km × 27 km horizontal resolution was employed in the study domain (Fig. S1), which covers Northeast Asia (100°E–150°E longitude, 20°N–50°N latitude) with 174 (W–E) × 128 (S–N) grid points and 15 vertical layers. The horizontal resolution was settled considering domain and objective of this study. According to previous studies (e.g., Gao et al., 2015, 2017), the aerosol feedback on meteorological fields was simulated well by WRF-Chem with horizontal resolution of 27 km. Initial and boundary conditions for the meteorological variables were obtained from 6-hourly 1° × 1° National Centers for Environmental Prediction (NCEP) Final Analysis (FNL) data (NCEP, 2000). The chemical boundary conditions for the main trace gases and particulate matter concentrations were provided by simulations by the Model for Ozone and Related Chemical Tracers (MOZART) (Emmons et al., 2010). In the chemical initial condition process, this study employed the model containing re-initialized NCEP meteorological fields for each day of a five-day run, recognized as sufficient for the initial conditions of chemical variables to reach equilibrium.

The anthropogenic emissions of sulfur dioxide (SO<sub>2</sub>), nitrogen oxides (NOx), carbon monoxide (CO), VOCs, black carbon (BC), organic carbon (OC), PM<sub>10</sub>, and PM<sub>2.5</sub> were based on MAPS-Seoul 2015 campaign emission data (Woo et al., 2014). This emission inventory

includes the Multi-resolution Emission Inventory of China (MEIC) (<http://www.meicmodel.org/>), Clean Air Policy Support System (C-APSS) (<http://airemiss.nier.go.kr>), and Regional Emission Inventory in Asia (REAS) version 2 (<http://www.jamstec.go.jp/frsgc/research/d4/emission.htm>). Biogenic emissions were calculated online using a model based on the Model of Emissions of Gases and Aerosols from Nature (MEGAN) inventory (Guenther et al., 2006). MEGAN has been fully coupled into WRF-Chem to enable the online calculation of biogenic precursor emissions subject to vegetation cover and meteorological conditions such as temperature and solar radiation at the time of the calculation (Grell et al., 2005). Dust, sea salt, and dimethylsulfide (DMS) emissions were not included in this study.

#### 2.4. Model experiments and case description

As a case study of the MAPS-Seoul 2015 campaign, two cases with warm cloud were selected. The simulations of these cases were run for 120 h with the first 24 h discarded as model spin-up for meteorology-chemistry interactions. Case A began at 00 UTC on 5 June 2015, and Case B started at the same time on 10 June 2015 (local time: UTC + 9 h).

To investigate the impact of aerosol effects on mesoscale meteorological fields, three experiments for the two cases were conducted: a control experiment (CTL) with no aerosol effects, an aerosol-radiation interaction experiment (ARI), and an aerosol-cloud-radiation interaction experiment (ACR). The CTL did not include any explicit aerosol-meteorology interactions and the ARI considered only radiative effects by including the aerosol direct effect on radiation without cloud effects. The ACR reflected the radiation effects of ARI plus additional aerosol-cloud interactions for grid-scale clouds. Therefore, the total (= direct + indirect) aerosol effects on meteorological fields were included in the ACR experiment. The differences in each experiment represent the direct effect, indirect effect, and total effect. For example, the difference between ACR and CTL (i.e., ACR - CTL) was to investigate the total aerosol effects, whereas the difference between ARI and CTL (i.e., ARI - CTL) and that between ACR and ARI (i.e., ACR - ARI) represented the aerosol direct and indirect effects, respectively. Table S3 summarizes the experiments.

Fig. 1 shows the meteorological and aerosol fields over specific 24-h periods for both case study periods. Fig. 1a and b shows the results of the ACR experiments from 12 UTC on 7 June (Case A), and Fig. 1c and d shows those from 00 UTC on 11 June (Case B). Fig. 1a and c shows the accumulated precipitation together with wind fields at 850 hPa, and Fig. 1b and d shows the total AOD at 550 nm and the liquid water path (LWP) at 500 hPa for both cases. Case A shows a high-pressure system over the eastern (China) and western (Japan) parts of the domain as well as a low-pressure system over the northern part (Fig. 1a). These pressure distributions led to a strong streamline through the East China Sea and East Sea of Korea with a southwesterly wind. In the modeled meteorological conditions of Case A, widespread precipitation of less than 15 mm day<sup>-1</sup> occurred near the Korean Peninsula. In Fig. 1b, a high simulated AOD value of more than 0.7 with clouds (LWP > 0.1 g m<sup>-2</sup>) was discovered over the southern region of the Korean Peninsula. Even though the region with clouds was excluded, the AOD was higher than 0.9 over the Yellow Sea. This indicates that the aerosol loading was transported to the Korean Peninsula via the Yellow Sea during the period of Case A. Case B is characterized by continuous westerly winds from China to the downwind regions under the influence of a cyclone system centered on the Northeast China region in Manchuria (Fig. 1c). Compared with Case A, minimal precipitation of < 10 mm day<sup>-1</sup> was simulated over South Korea. As the transport process of air mass from China progressed, high aerosol loadings were clearly detected over the Korean Peninsula (Fig. 1d).

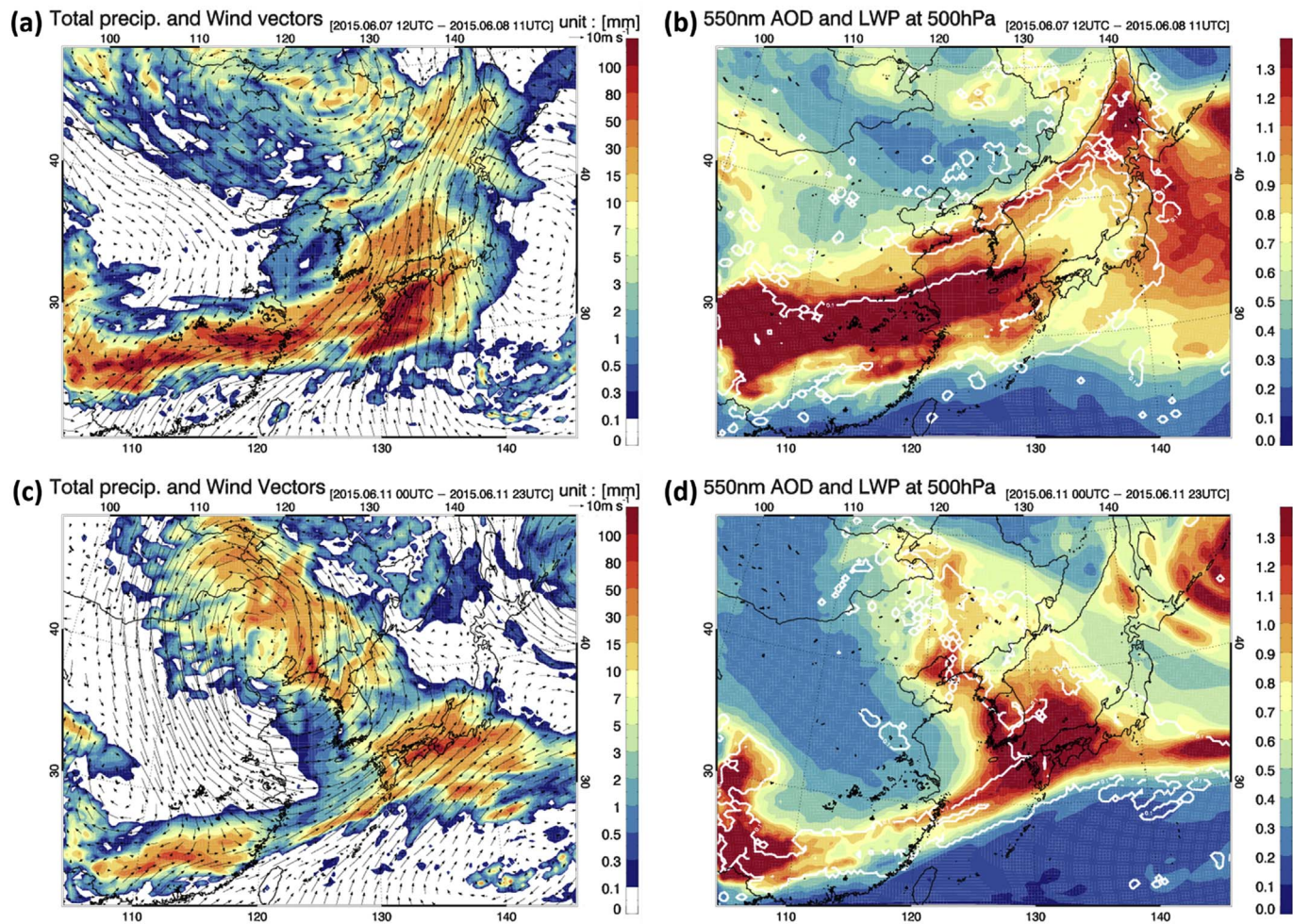


**Fig. 1.** Spatial distributions of (a) total precipitation (color, in  $\text{mm day}^{-1}$ ) and temporally averaged wind vectors (arrows, in  $\text{m s}^{-1}$ ) at 850 hPa and (b) temporally averaged column aerosol optical depth (AOD) at 550 nm (color) and liquid water path (LWP) at 500 hPa (white contours, in  $\text{g m}^{-2}$  above  $0.1 \text{ g m}^{-2}$ ) from the aerosol-cloud-radiation interaction (ACR) experiment for Case A (12 UTC on 7 June 2015 to 11 UTC on 8 June 2015). Panels (c) and (d) are the same as (a) and (b), but for Case B (00 UTC on 11 June 2015 to 23 UTC on 11 June 2015).

### 3. Results

#### 3.1. Model evaluation

To verify the model's representation of our aerosol-cloud-radiation feedback experiment, model performance was evaluated by comparing the simulated meteorological variables and aerosol loadings against surface, aircraft measurements, and satellite data. Table 1 provides a statistical summary of the comparisons for meteorological variables including temperature, relative humidity (RH), and wind speed for the ACR experiments for both cases. The model depicted the temperature and its temporal variation with a Corr. R of 0.93–0.94 and an MB of  $-1.38$  to  $-0.95$  °C. RH was also reasonably reproduced with Corr. R values of 0.86–0.93 and MB of 8.95–10.47. The simulated wind speed agreed well with the observation of Corr. R = 0.70 to 0.77, but was systematically overestimated for Case A with an NMB of 112%. Noted that in previous studies, a high positive bias (e.g., NMB of 78.1–105%) in wind speed was often obtained in WRF-Chem simulations (Matsui et al., 2009; Zhang et al., 2010; Molders et al., 2012; Tuccella et al., 2012; Gao et al., 2015; Zhang et al., 2015). This high bias is partly attributed to unresolved topographical features in surface drag parameterization and the coarse resolution which were all previously studied (Cheng and Steenburgh, 2005; Yahya et al., 2015; Zhang et al., 2015).

Observed and simulated precipitation rates (PR) were estimated at

three sites, namely Gosan, Jinju, and Incheon, where precipitation was observed during the study periods (Fig. 2). The model results overestimated the PR for all experiments. However, the results of the model for ACR experiment led to higher threat score values of 0.25–0.29 with an NMB reduction of about 25% compared to the CTL and ARI experiments. Furthermore, the onset detection of PR demonstrated a time lag for the ACR experiment compared to other experiments, with a delay of onset time of 9 and 2 h at Gosan and Jinju, respectively. In addition, the peak time of PR also demonstrated a time lag with a delay of 9 and 4 h at Gosan and Jinju, respectively (Fig. 2a and b). This suggests that the ACR experiment, with full aerosol feedback effects, simulated a higher probability of precipitation than the other experiments. Fig. 3 indicates the spatial distributions of the PR, showing a stronger similarity to the distribution of the TRMM product in the ACR. In the ACR experiment, the PR was less intense and covered a smaller area over the Korean Peninsula at 21 UTC on 7 June. And the shape of the precipitation band had similar patterns to the TRMM observation at 21 UTC on 11 June (Fig. 3). The analysis above indicates that the ability to simulate precipitation, including the presence and rate of precipitation improved in the ACR experiment.

To investigate the chemical compositions of the aerosols in detail, the aircraft measurements of RF7 for Case B were compared with those of RF4 for Case A. Here, noted that the flight paths of RF4 and RF7 were similar, with the aircraft traveling to Seoul (Fig. S1). Fig. S2 shows that  $\text{PM}_{2.5}$ , sulfate, and ammonium for RF4 were simulated well, whereas

**Table 1**

Statistics of the comparisons between simulated and observed temperature ( $^{\circ}\text{C}$ ), relative humidity (RH, %), and wind speed ( $\text{m s}^{-1}$ ) for Case A (00 UTC 6 June to 23 UTC 9 June) and Case B (00 UTC 11 June to 23 UTC 14 June), respectively.

	Case A (00UTC 6 June to 23UTC 9 June)			Case B (00UTC 11 June to 23UTC 14 June)		
	Temp. ( $^{\circ}\text{C}$ )	RH (%)	WS ( $\text{m s}^{-1}$ )	Temp. ( $^{\circ}\text{C}$ )	RH (%)	WS ( $\text{m s}^{-1}$ )
MEAN OBS <sup>a</sup>	20.41	69.46	1.77	22.08	73.64	2.20
MEAN MOD <sup>b</sup>	19.46	79.93	3.75	20.70	82.59	4.34
Corr. R <sup>b</sup>	0.93	0.86	0.70	0.94	0.93	0.77
MB <sup>c</sup>	-0.95	10.47	1.98	-1.38	8.95	2.14
NMB <sup>d</sup>	-4.65%	15.07%	112.28%	-6.26%	12.15%	97.26%
NME <sup>d</sup>	6.52%	15.76%	112.28%	6.58%	12.15%	97.26%
FB <sup>e</sup>	-4.65%	14.65%	74.67%	-6.78%	11.55%	67.69%
FE <sup>e</sup>	6.90%	15.28%	74.67%	7.09%	11.55%	67.69%
RMSE <sup>f</sup>	1.55	13.09	2.09	1.73	10.51	2.24
IOA <sup>g</sup>	0.94	0.82	0.45	0.91	0.88	0.45

<sup>a</sup> MEAN OBS and MEAN MOD are hourly mean values of observation and model results, respectively.

<sup>b</sup> Corr. R the correlation coefficient between the observation and model results.

<sup>c</sup> MB the mean biases.

<sup>d</sup> NMB and NME the normalized mean bias and error.

<sup>e</sup> FB and FE the fractional bias and error.

<sup>f</sup> RMSE the root-mean-square error.

<sup>g</sup> IOA the index of agreement.

those for RF7 were slightly underestimated at about 15, 5, and  $1 \mu\text{g m}^{-3}$  for each of the three chemical components, respectively. This suggests that the lack of formation mechanisms of secondary inorganic aerosols, such as the heterogeneous reaction of  $\text{SO}_2$  on the surface (Harris et al., 2013), is a possible reason for the underprediction. The modeled OA was significantly underestimated for both RF4 and RF7 flights, although OA had a larger fraction of total mass for the aircraft measurements. The capability of OA forecasting of the WRF-Chem is suggested as a reason for underestimation. Therefore, with the exception of OA, the overall simulated aerosol mass could be reasonably compared quantitatively to observed values.

### 3.2. Aerosol effects on radiative variables

To evaluate how well the WRF-Chem model simulated the impact of aerosol feedback on mesoscale meteorological fields, the radiation-cloud variables were analyzed. The three experiments were investigated by two different sky conditions: clear-sky and all-sky as in a previous study (Archer-Nicholls et al., 2016). The clear-sky variables were calculated for the grid points with no clouds, yielding results without the influence of clouds in the model. The all-sky condition denotes a clear sky plus cloudy sky conditions. To compare the radiation-cloud variables with the corresponding modeled aerosol loading, the resultant vertical profiles of the extinction coefficient at 550 nm over South Korea for the two cases in the ACR experiment were examined.

Fig. 4 shows a time series of various aerosol effects on downward shortwave (SW) radiation in clear- and all-sky conditions for both cases at ground level averaged across South Korea. In the case of clear-sky conditions, as indicated in Fig. 4a and b, the total effects on the changes in downward SW radiation at the ground (denoted as  $\Delta SW_{\text{fc},\text{clr}}^{\downarrow}$ ), with maximum values of  $-112.2$  and  $-144.6 \text{ W m}^{-2}$  for Case A and Case B, originated mostly from direct effects. As expected, only small indirect effects of  $\sim 26.2 \text{ W m}^{-2}$  at 07 UTC on 8 June (Fig. 4a) and  $\sim 50.1 \text{ W m}^{-2}$  at 06 UTC on 11 June (Fig. 4b) were found for Case A and Case B, respectively. However, in the all-sky condition, the radiative variables with cloud fields tended to change more dramatically than in the clear-sky condition. In Fig. 4c and d, the more sharply

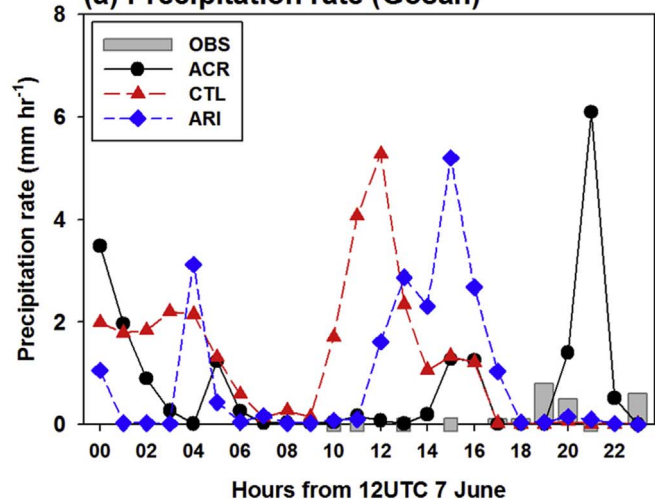
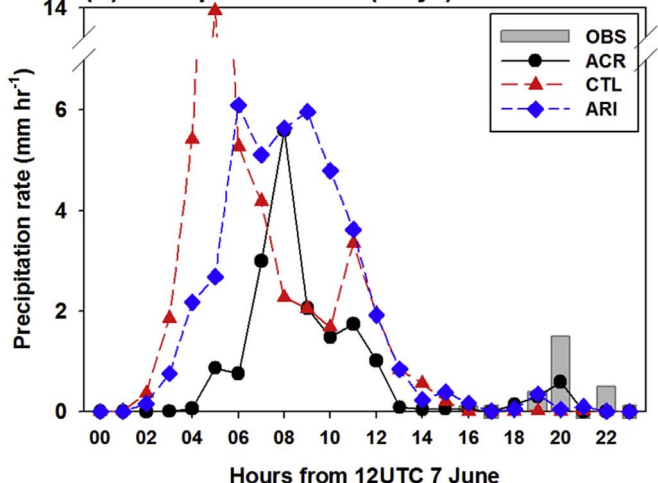
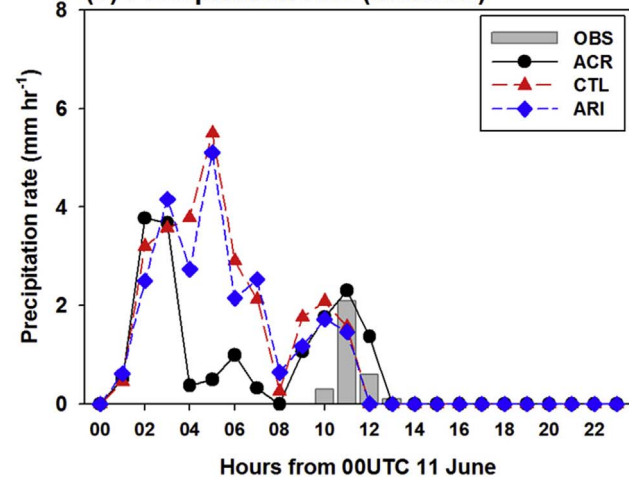
**(a) Precipitation rate (Gosan)****(b) Precipitation rate (Jinju)****(c) Precipitation rate (Incheon)**

Fig. 2. Time series of observed (gray bar) and simulated hourly precipitation rate ( $\text{mm hr}^{-1}$ ) at (a) Gosan and (b) Jinju for Case A and (c) Incheon for Case B. The black circles represent the aerosol-cloud-radiation interaction (ACR) experiments, red triangles indicate the aerosol-radiation interaction (ARI) experiments, and blue diamonds show the control (CTL) experiments. (For interpretation of the references to colour in this figure legend, the reader is referred to the web version of this article.)

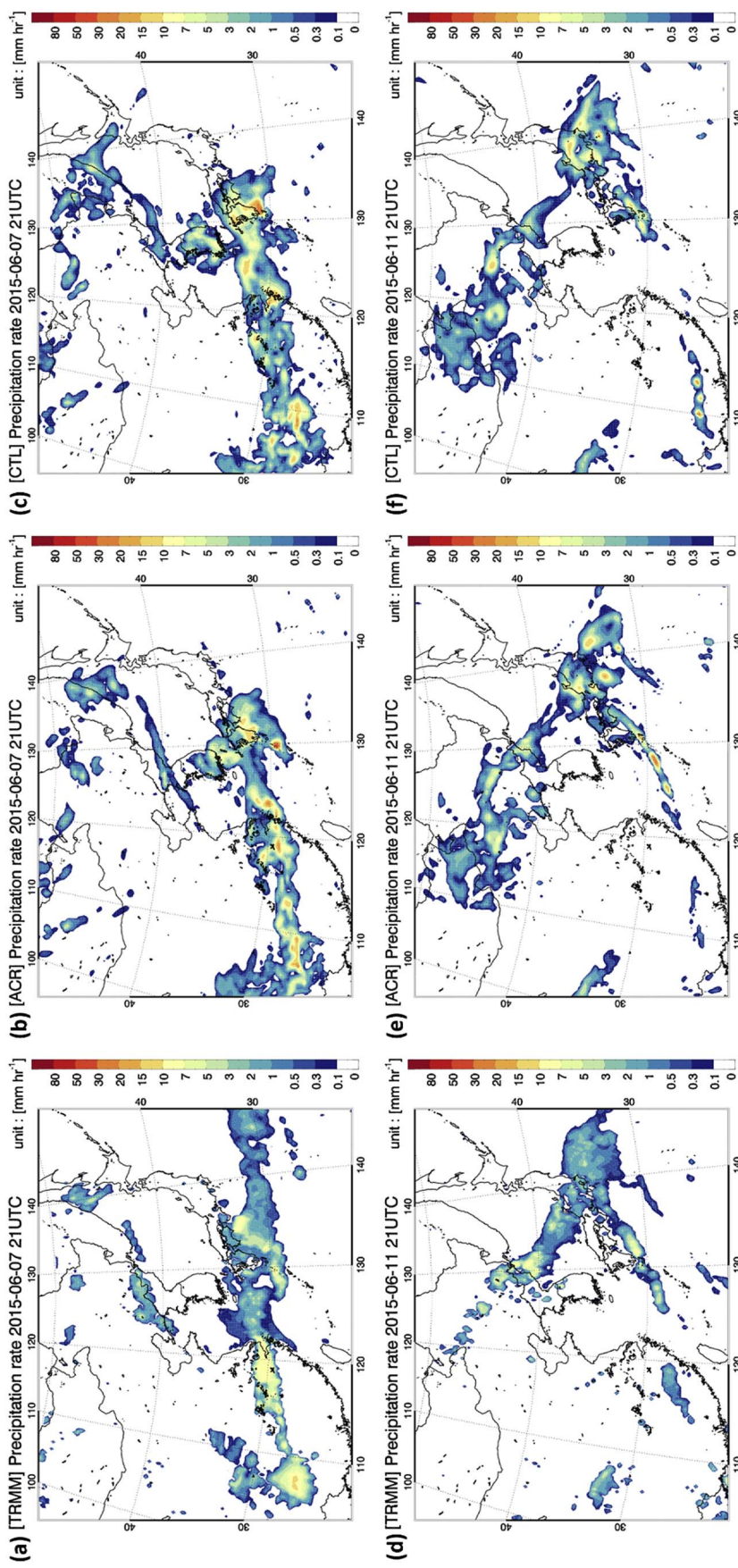
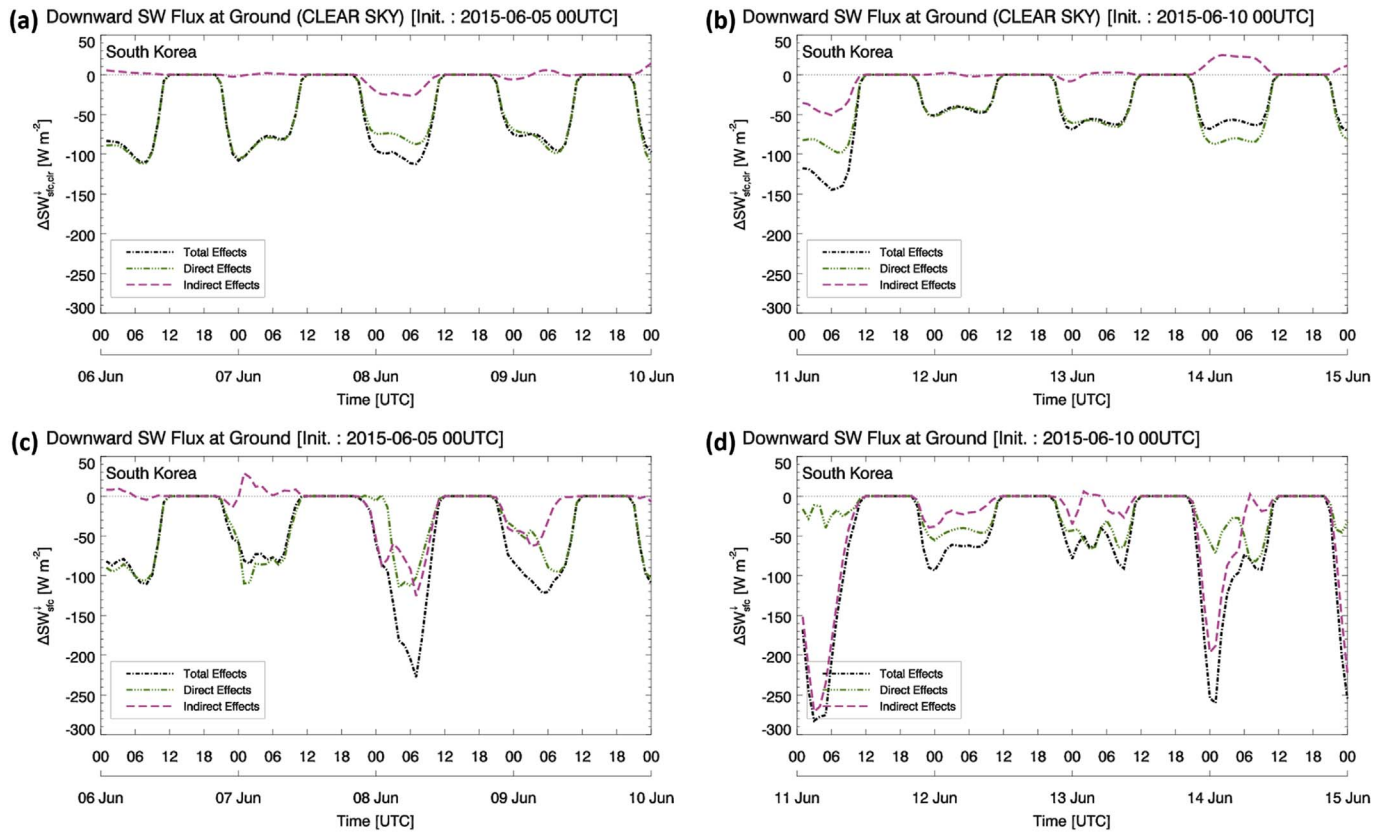


Fig. 3. Spatial distributions of precipitation rate ( $\text{mm hr}^{-1}$ ) from (a) Tropical Rainfall Measuring Mission (TRMM) data, (b) the aerosol-cloud-radiation interaction (ACRI) experiment, and (c) the control (CTL) experiment at 21 UTC on 7 June 2015 for Case A. Panels (d)–(f) are the same as (a)–(c), respectively, but at 21 UTC on 11 June 2015 for Case B.



**Fig. 4.** Time series of change in downward shortwave (SW) radiation averaged at the ground level over South Korea for (a) Case A and (b) Case B in clear-sky conditions. Panels (c) and (d) are the same as (a) and (b), respectively, but for all-sky conditions.

reduced downward SW radiation shown in the all-sky condition (denoted as  $SW_{sfc}^{\downarrow}$ ) is mostly attributed to the indirect effects, especially for Case B. This difference between direct and indirect effects was more obvious at 03 UTC on 11 June for Case B with  $-11.4 \text{ W m}^{-2}$  ( $-1.8\%$  against CTL) for direct effects, but  $-271.0 \text{ W m}^{-2}$  ( $-42.6\%$  against CTL) for indirect effects, where cloud fraction (CF) of up to 40% was simulated.

Whereas almost sinusoidal daily variations in direct effects contributed for both clear- and all-sky conditions, indirect effects demonstrated more intermittent patterns with sharply increased contributions depending on CF for all-sky conditions. For example, the maximum decrease of  $SW_{sfc}^{\downarrow}$  in the indirect effects including cloud impact were simulated as  $-125.5$  to  $-271.0 \text{ W m}^{-2}$  ( $-23.1$  to  $-42.6\%$ ) for Case A and Case B, respectively (Fig. 4c and d). At the same time, the gaps between  $\Delta SW_{sfc,clr}^{\downarrow}$  and  $\Delta SW_{sfc}^{\downarrow}$  reached  $99.3 \text{ W m}^{-2}$  (20.1%) and  $220.1 \text{ W m}^{-2}$  (36.7%) for the two cases, respectively.

Fig. 5 illustrates the vertical profiles of the extinction coefficient for both cases, showing some agreement compared to the variation in  $SW_{sfc,clr}^{\downarrow}$  and  $SW_{sfc}^{\downarrow}$ . The radiative variables are attributed mainly to the scattering and absorption of solar radiation. The reduction of downward SW radiation by aerosol varies as amount of solar radiation begin to deviate after sunrise, and in turn tends to change more dramatically by the presence of high aerosol loadings. The results changed drastically in  $SW_{sfc}^{\downarrow}$  reaching up to  $-271.0 \text{ W m}^{-2}$  when the extinction coefficient was more than  $0.22 \text{ km}^{-1}$  near the surface. This indicates that the reduction of downward SW radiation by aerosols is associated with the extinction coefficient profile directly and indirectly, particularly in conditions of high aerosol loading.

Regarding upward SW radiation at the ground (denoted as  $SW_{sfc}^{\uparrow}$ ), it is known that the portion of incoming radiation is reflected at the surface and strongly dependent on the surface albedo. This study obtained the same results. However, we also determined that the simulated  $\Delta SW_{sfc,clr}^{\uparrow}$  and  $\Delta SW_{sfc}^{\uparrow}$  were approximately 15% (or less) of

$\Delta SW_{sfc,clr}^{\downarrow}$  and  $\Delta SW_{sfc}^{\downarrow}$  with the same temporal variations.

In this study, we excluded the change in upward longwave (LW) radiation by aerosol, because no significant biases were found. In general, upward LW radiation in the clear-sky condition (denoted as  $LW_{sfc,clr}^{\uparrow}$ ) at the ground depends mostly on the changing skin temperature based on the Stefan-Boltzmann law as a function of the variations in solar radiation (Stefan, 1879; Boltzmann, 1884). The modeled  $LW_{sfc,clr}^{\uparrow}$  was in phase with the surface skin temperature. In our WRF-Chem simulations, the LW radiation change between the all-sky condition (denoted as  $LW_{sfc}^{\uparrow}$ ) and  $LW_{sfc,clr}^{\uparrow}$  was small and negligible (not shown).

Fig. 6a and b shows the time series of the differences in downward LW radiation at the ground averaged across South Korea for both cases. As shown in Fig. 6a and b, the total effects on downward LW radiation at the ground (denoted as  $LW_{sfc}^{\downarrow}$ ) were similar to the indirect effects, whereas the direct effects were small and negligible with a difference of  $-6.5$  to  $+8.1 \text{ W m}^{-2}$  ( $-1.8$  to  $+2.6\%$ ) for Cases A and B. The total aerosol effects can lead to large increases in  $\Delta LW_{sfc}^{\downarrow}$  with maximum values of  $30.8$  to  $51.8 \text{ W m}^{-2}$  (9.7 to 15.0%) for both cases, whereas the averaged values across South Korea ranged from  $-7.2$  to  $+10.5 \text{ W m}^{-2}$  ( $-1.9$  to  $+2.7\%$ ).

To analyze the total effects in interpreting the changes in  $LW_{sfc}^{\downarrow}$ , cloud parameters were examined in this study. Fig. 6c and d illustrates the cloud water mixing ratio (QCLOUD) for both cases. In Fig. 6c and d, the variation of QCLOUD was seen extensively by the high aerosol loading through the process of aerosol-cloud interaction. Upon the condition of all large increases of  $\Delta LW_{sfc}^{\downarrow}$  with a maximum value of  $51.8 \text{ W m}^{-2}$  (15.0%), significant growth in cloud formation was found particularly in the condition of  $\Delta QCLOUD$  exceeding  $110 \text{ mg kg}^{-1}$ , particularly at altitudes below 950 hPa (Fig. 6c and d). This is suggesting the increased QCLOUD reflecting the LW radiation, especially at near the surface. Therefore, a portion of LW radiation emitted from the surface is trapped by low-level clouds, resulting in radiative warming at

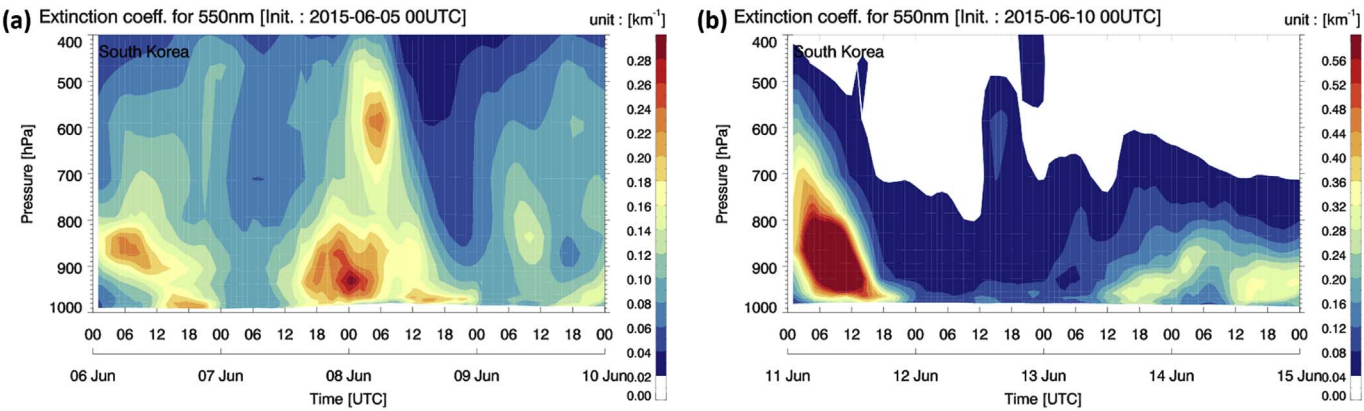


Fig. 5. Simulated vertical profiles of extinction coefficient at 550 nm from the aerosol-cloud-radiation interaction (ACR) experiment averaged over South Korea for (a) Case A and (b) Case B.

the ground. However, the magnitude of  $\Delta L W_{\text{sf}}^{\downarrow}$  was determined as relatively small compared to  $\Delta S W_{\text{sf}}^{\downarrow}$ .

### 3.3. Aerosol effects on clouds and precipitation

To investigate the manner in which aerosol-cloud-radiation interaction affects the cloud microphysics of the atmosphere, the associated CF and PR were analyzed. Fig. 7 displays the time series of CF and PR averaged over South Korea for the three experiments. Of the three experiments, the simulated CF showed the highest values in the ACR experiment for both cases. The direct effects contributed to CF values of  $-6.7\%$  to  $3.8\%$ , whereas the indirect effects significantly increased in CF difference (ACF) up to  $22.7\%$  (Fig. 7b and f), controlling the cloud lasting time. This indicates the importance of the second indirect effects

associated with changing the cloud cover and cloud lifetime.

Our study also correlated the difference in CF by indirect effects with that of low-level QCLOUD, as shown in Fig. 6c and d. Comparing Fig. 4c and d to Fig. 7b and f strongly associated the phase of indirect effects on CF and other cloud variables such as QCLOUD with the radiative variables. This implies that the perturbation in radiation properties yields cloud formation involving indirect effects and vice versa; therefore, the interaction of clouds and radiation properties is undoubtedly significant in the prediction of cloud cover and amount.

In Fig. 7d and h, the fluctuation in PR by aerosol effects was shown to occur at a similar period when CF was increased by the total effects, but showed a relatively low correlation with cloud variations, likely because of nonlinear cloud to precipitation conversion processes. As shown in Fig. 7c and g, the ACR experiment decreased precipitation

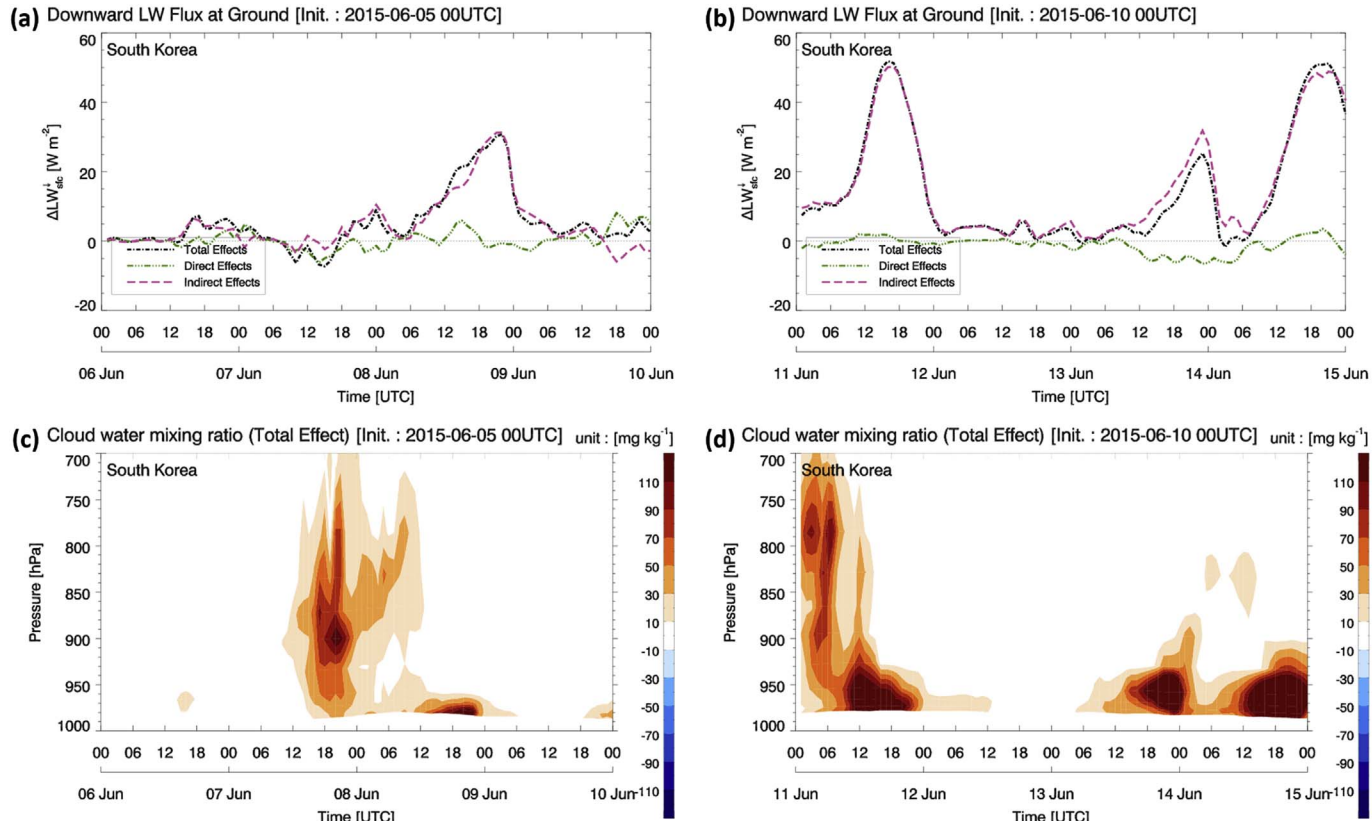
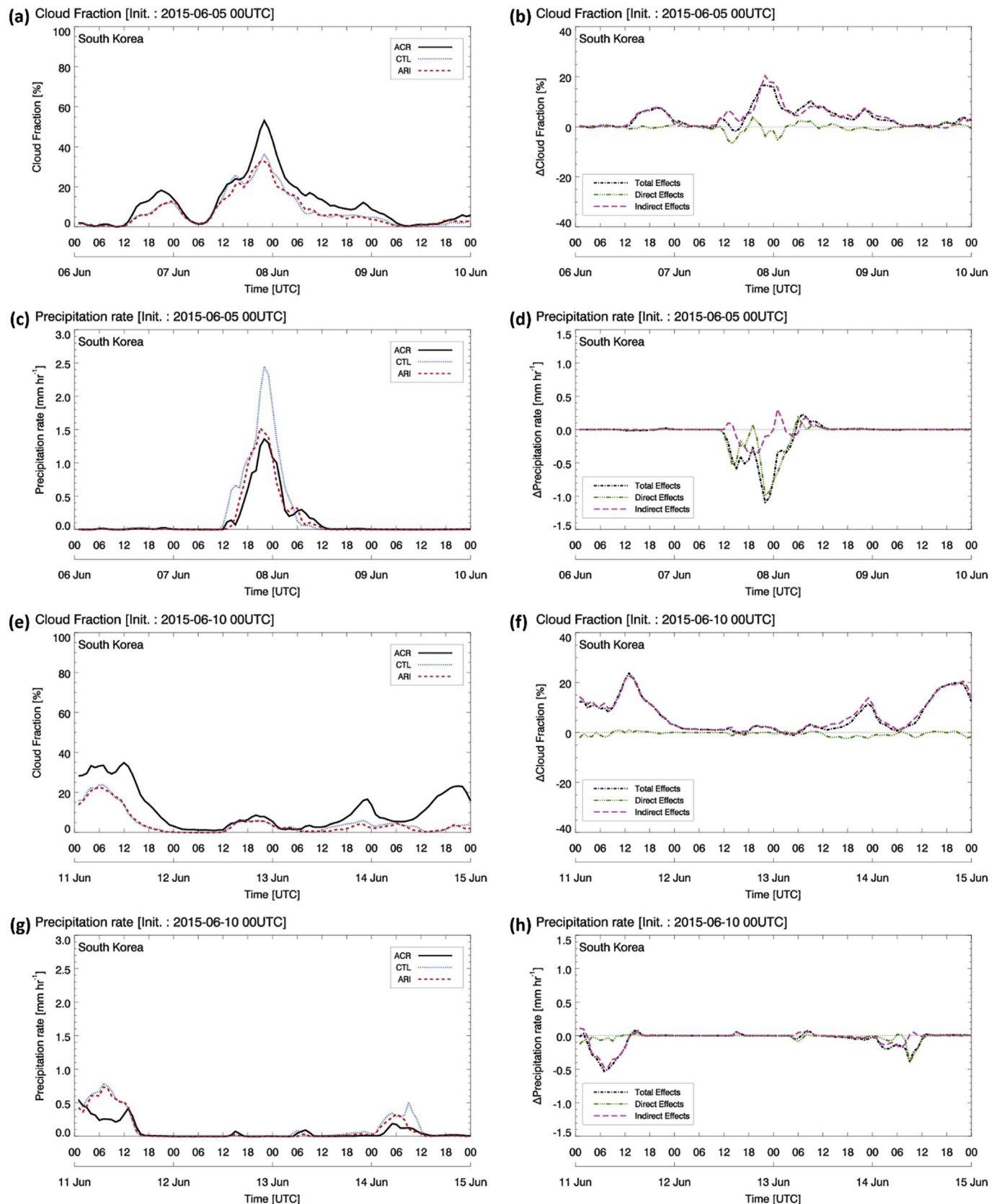


Fig. 6. Time series of change in downward longwave (LW) radiation averaged at the ground level over South Korea for (a) Case A and (b) Case B in all-sky conditions. Panels (c) and (d) show simulated vertical profiles of total effects on the cloud water mixing ratio (QCLOUD) averaged over South Korea for Case A and Case B, respectively.



**Fig. 7.** Time series of cloud fraction (CF) and precipitation rate (PR) averaged over the South Korea. Panel (a) CF for three experiments; panel (b) difference of CF in aerosol effects of total, direct, and indirect effects; panel (c) PR simulated from three experiments, (d) difference of PR from aerosol effects for Case A. Panels (e)–(h) are the same as (a)–(d), respectively, but for Case B.

more than other experiments. This result is consistent with those from observed PR, as illustrated in Fig. 2. Fig. 2 indicates that the ACR experiment better agreed with observations, especially at Gosan, implying that aerosol-cloud-radiation interaction is an important factor for improving daily weather prediction of precipitation. Similar results are reported by numerous studies that performed an inter-comparison of coupled chemistry-meteorology models over Europe, such as Forkel et al. (2012), Brunner et al. (2015), and Kong et al. (2015). Their studies considered the importance of aerosol, cloud, and radiation interaction, validating that the simulation with aerosol feedback more accurately reproduced microphysical variables and incoming downward SW radiation.

Fig. S3 illustrates the mean spatial distributions of LWP simulated from the ACR experiment and its attribution fraction of aerosol total effects over specific 24-h periods of the two cases. Here, Figs. S3a and S3c represent LWP ( $\text{g m}^{-2}$ ), and Figs. S3b and S3d illustrate the contribution fraction of total effects to LWP, respectively. As shown in Fig. S3, cloud formation occurred mainly over Southeast and East China, the Korean Peninsula, and East China Sea (Figs. S3a and S3c). In Figs. S3b and S3d, the LWP showed a spatially increased pattern nearly proportional to the LWP by the total aerosol effects, mostly due to indirect effects. The LWP was greatly augmented to 614.8 and  $518.9 \text{ g m}^{-2}$  for Cases A and B, respectively. This implies that the simulated LWP was influenced by aerosol indirect effects, as shown in Fig. 7b and f, which alter cloud properties such as liquid water content, CF and cloud lifetime.

These augmentations in LWP can be attributed to the increase in the droplet number mixing ratio (QNDROP), which was derived from the higher number of particle concentrations in the ACR experiment. The CTL and ARI experiments did not consider the activation of aerosol-originated cloud droplet number source; therefore, the QNDROP without aerosol-cloud interaction was significantly lower than that in ACR experiment. However, previous studies such as by Zhang et al. (2015) and Forkel et al. (2015) showed that aerosol-cloud interaction reduces QNDROP, because of almost horizontally homogeneous particle numbers and the QNDROP calculated for unpolluted conditions. The process described above yields different results for cloud-precipitation than those determined in the present study. The discrepancy between previous studies and this research is attributed to the different environment of aerosol characteristics. Our domain, which includes highly polluted areas, represents distinctly different physical and chemical aerosol characteristics under abundant cloud water content conditions. For example, Forkel et al. (2015) showed the result of indirect effects in unpolluted marine or coastal area, while Zhang et al. (2015) focused on a low cloud cover region and a season dominated by direct effects. That is, a more adequate quantity of data on aerosol characteristics is a prerequisite to diagnose the relationship between aerosol effects and cloud variables. Furthermore, it can partly be explained by the different version of the aerosol-cloud feedback mechanism of WRF-Chem. In the detailed WRF-Chem model (i.e., version 3.6), better performance becomes possible for more realistic aerosol fields and aerosol-cloud interaction under the various and different conditions of aerosol concentrations.

Last, we examined the manner in which the increased LWP affects precipitation in and around the Korean Peninsula. Fig. 8 displays the spatial distributions of total, direct, and indirect effects on precipitation for both cases. Here, total precipitation is indicated in Fig. 1a and c. In Fig. 8, the changes of aerosol effects on precipitation occur predominantly in regions such as the southeastern and central parts of Korean Peninsula for Case A and Case B, respectively, where the LWP is distinctly increased by aerosol effects. The spatial distribution of changes in precipitation demonstrated continuously iterated patterns of decrease and increase, which were also reported by Mashayekhi and Sloan (2014).

Considering the overall spatial distribution of aerosol effects, a distinct difference is evident between Case A and Case B. Direct and

indirect effects equally contributed to the total effects on the variation of precipitation for Case A. Whereas, in Case B, a more dominant contribution of indirect effects than direct effects was evident. For example, for Case A, the direct effects on changes in precipitation over South Korea, ranging from  $-54.6\text{--}+24.1 \text{ mm}$ , were comparable to those of indirect effects, ranging from  $-23.8\text{--}+24.0 \text{ mm}$ , and almost equally contributed to the total effects with values ranging from  $-63.2\text{--}+27.1 \text{ mm}$  (Fig. 8a–c). In contrast, the direct effects for Case B, with a minimum value of  $-7.0 \text{ mm}$ , had little influence on the changes in precipitation compared to the indirect effects, with a minimum value of  $-36.6 \text{ mm}$  (Fig. 8d–f). The characteristics of each case correspond to the averaged  $\Delta\text{PR}$  over South Korea, as shown in Fig. 7d and h. For Case A, the time series of  $\Delta\text{PR}$  by direct effects was more dominant, followed by total effects (Fig. 7d). For Case B, the phase of  $\Delta\text{PR}$  derived from indirect effects with relatively little direct effects (Fig. 7h).

To further explain and obtain better insight into the differences between the two cases, we demonstrated that both (=direct + indirect) effects are dominant, and only indirect effects are dominant on precipitation for the conversion of cloud water to rain. We analyzed the longitude-height cross section of the difference in the tendency for the conversion of cloud water to rain (Fig. 9). The differences in wind fields averaged over specific 24-h periods for both cases are indicated in Fig. 9. For both cases, the precipitation system propagated from the southwest (or west) toward the northeast, passing through the Korean Peninsula. In Fig. 9a and e, over the upstream (West) area, total effects on the cloud water to rain conversion showed a negative (–) sign for both cases, indicating that aerosol effects suppress precipitation. However, a positive sign (+) for Case A was simulated over the downstream (East) area (Fig. 9a and e).

The variations in direct effects shown in Fig. 9b can be explained by vertical wind fields, which vary according to meteorological variables such as upward motion due to radiation, temperature, and stability/convection of the atmosphere in Case A. That is, radiative direct cooling over the near-surface high aerosol concentration area induces a sinking motion (see wind vector perturbations in Fig. 9b) due to the decreased surface temperature (Fig. 4c), enhancing stable stratification of the suppression process of the cloud water into rain conversion. As illustrated in Fig. 4c, the  $\Delta SW_{\text{sf}}^{\downarrow}$  for direct effects significantly influences on the reduction in  $SW_{\text{sf}}^{\downarrow}$ , because of the total effects for Case A. The decrease of radiation reaching the ground is reflected in the perturbation of temperature, which results in variation of atmospheric stability and convection processes. Following Zhao et al. (2012), because aerosol-induced warming or cooling accumulates over time, the temperature pattern does not accurately match the anomalies of vertical motion. Hence, it should be noted that the change of vertical velocity is not directly comparable to that of temperature, although the wind field varies with the temperature. In Case B, however, the radiative flux convergence was little simulated with no significant changes of vertical motions over the study domain.

The indirect effects on change in precipitation with the alteration of cloud properties by acting as the CCN were also investigated, as shown in Fig. 9c and g. The indirect effects suppressed precipitation over the upstream areas for both cases, and the results correspond to the distributions of cloud variables (Figs. S3b and S3d). This suggests that indirect effects over Northeast Asia can suppress the PR and resultantly delay the onset of precipitation. Interesting here is the opposite tendency over the downstream area for Case A (Fig. 9c), although no significant sign was found in Case B (Fig. 9g). In Case A, the time-mean RH was predominantly high (RH > 85% at altitude below 1.5 km), as shown in Fig. 9d, where abundant water vapor was favorable for saturation. Therefore, vapor condensation invokes adiabatic warming, directly inducing an enhanced updraft motion, as indicated in Fig. 9c and d. This process ultimately enhances the fluctuations of precipitation in these conditions. In contrast, the RH in Case B is lower than 75%, except for near the surface (Fig. 9h), where there was little saturation-

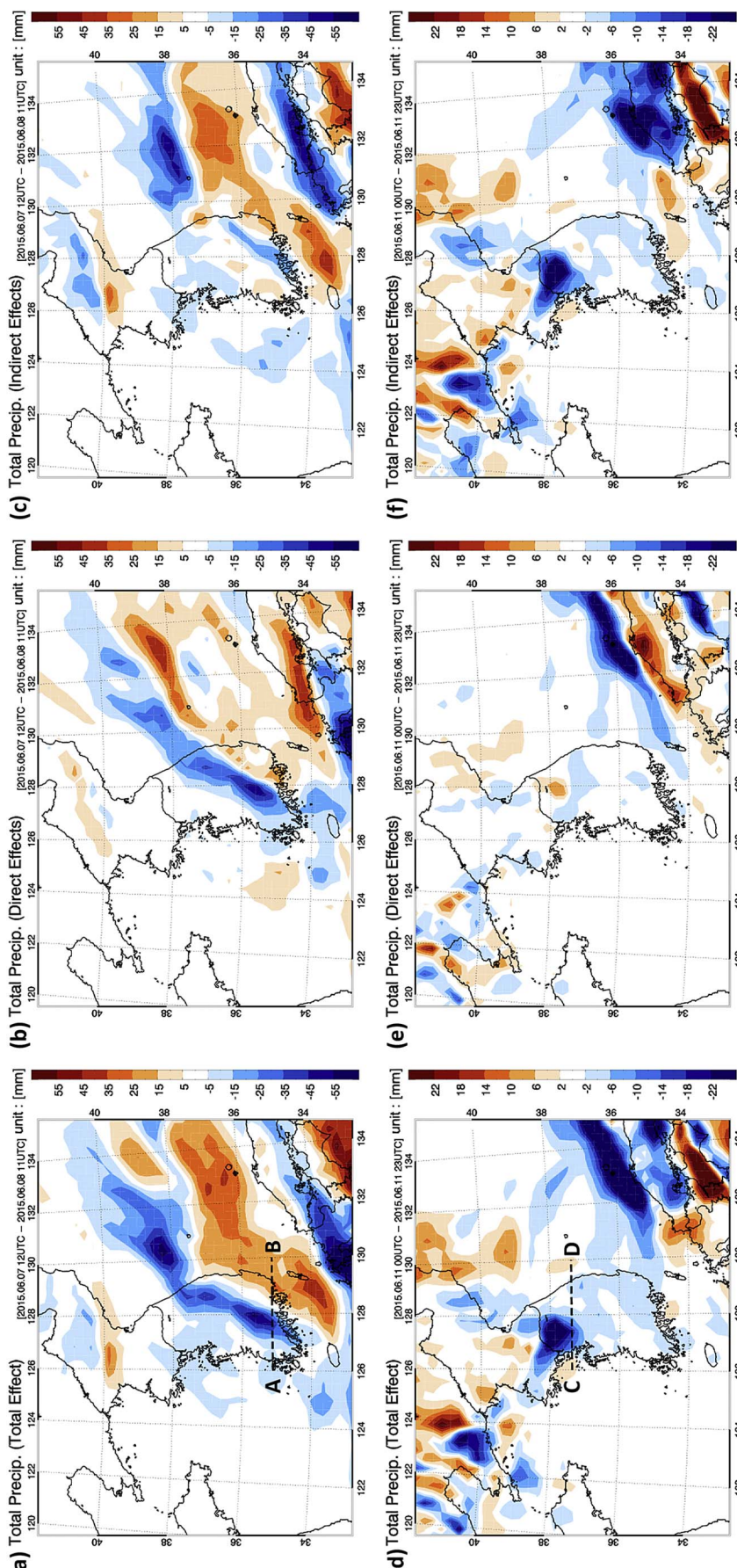


**Fig. 8.** Spatial distributions of temporally averaged (a) total effects, (b) direct effects, and (c) indirect effects on total precipitation for Case A. Panels (d)–(f) are the same as (a)–(c), respectively, but for Case B. Line AB and CD denote the cross section to be used in Fig. 9.

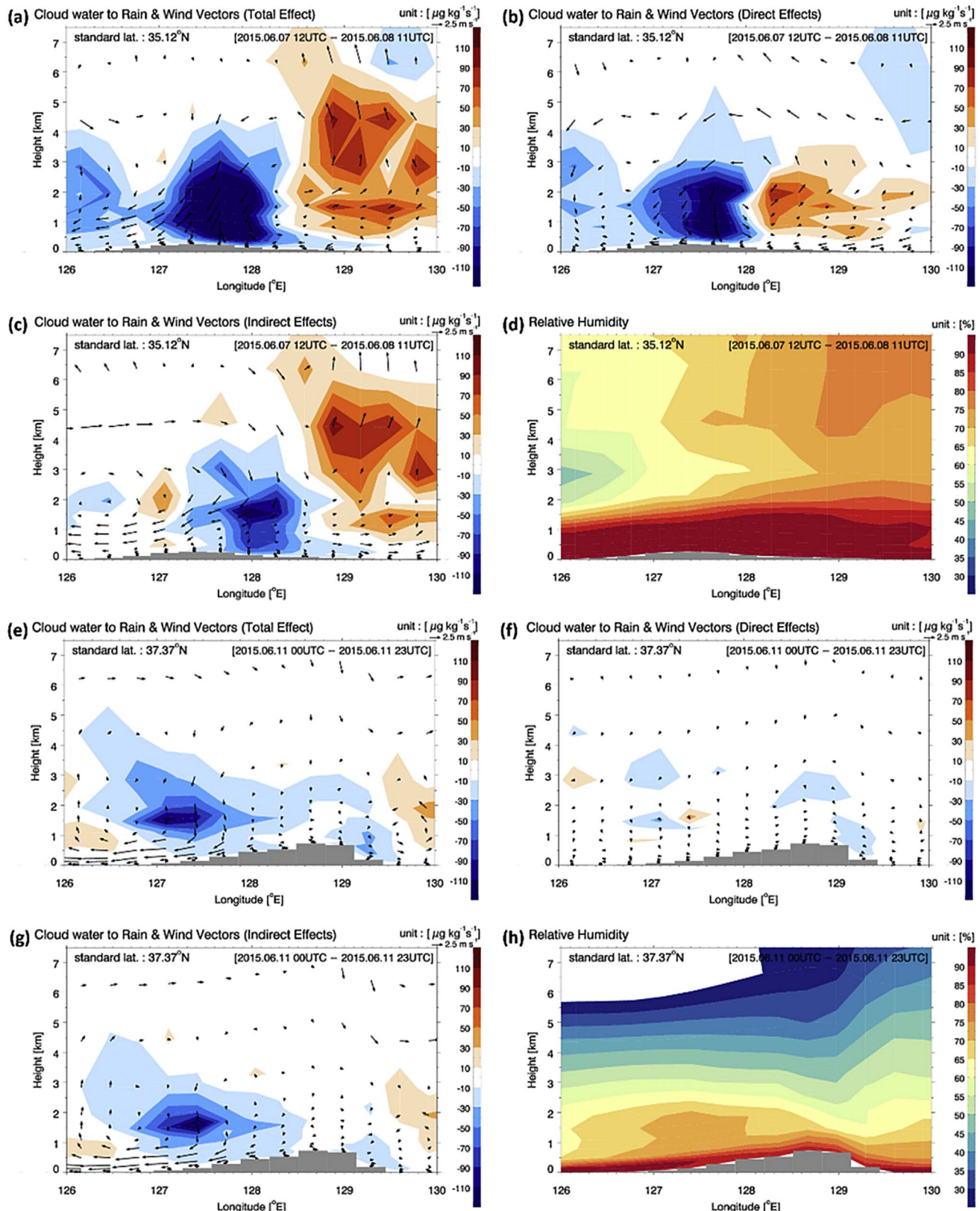


**Fig. 9.** Longitude-height cross section of (a) total effects, (b) direct effects, and (c) indirect effects on tendency for conversion of cloud water to rain (color, in  $\mu\text{g kg}^{-1}\text{s}^{-1}$ ) and wind fields (arrow, in  $\text{m s}^{-1}$ ), and (d) relative humidity (RH) for the aerosol-cloud-radiation interaction (ACR) experiment for Case A. Panels (e)–(h) are the same as (a)–(d), respectively, but for Case B. Note that the vertical wind speed was multiplied by a factor of 100.

warming thermodynamic processes and therefore a relatively smaller (or no) increase in cloud to precipitation conversions over the downstream (East) area in Case B.

Obviously, clouds are highly nonlinear systems and cloud-radiation environments can yield unpredictable results that create challenges in the interpretation of simulated and observed data. Furthermore, the current analysis is not sufficient to completely describe aerosol effects, because the aerosol activation process employed here cannot consider IN for the aerosol scheme (i.e., MADE/SORGAM) used in the current version of the WRF-Chem study. This indicates that the tendency towards possible underestimation in quantifying the role of indirect effects should be explored in the modeling study. To represent aerosol effects more accurately and quantitatively, it is therefore necessary to perform further modeling and employ more compressive measurements for ice-borne aerosols and IN treatment.

#### 4. Summary and conclusions

The main objectives of this study were to characterize and diagnose the influences of aerosol effects on mesoscale cloud-radiation variables over Northeast Asia during the MAPS-Seoul 2015 campaign period. We employed the fully coupled online WRF-Chem model and three different experiments with and/or without aerosol effects were carried out for the investigation of aerosol-cloud-radiation interaction.

The numerical results were first evaluated against available measurements obtained from MAPS-Seoul 2015 campaign, and we clearly found out that a case with full aerosol feedback effects yielded better prediction capability than other two experiments. It is also noted that the aerosol effects played a dominant role in altering radiative variables and cloud properties over downstream areas. The largest difference among the radiative variables due to aerosol effects was in downward SW radiation. The resultant perturbation in radiation properties was highly likely to be associated with the aerosol loading profile, and in turn involved in the cloud response. This is suggesting that the interaction between cloud and radiation was significant in the prediction of cloud cover/amount. In addition, compared with the respective aerosol effects on cloud properties, the total effects are attributed to indirect effects. Also, the variations of cloud properties and precipitation by total effects occurred at almost the same time over South Korea. However, contribution fraction of respective aerosol effects on precipitation varied according to meteorological conditions. We realized that the nonlinear cloud to precipitation conversion process worked on the downstream area.

In addition, we pointed out that, under abundant cloud water and aerosol conditions, the direct and indirect effects locally suppressed the precipitation and resultantly delayed the onset of precipitation with the time lag of up to 9 h over Northeast Asia. This implies the importance of aerosol effects in improving mesoscale precipitation predictabilities in the high polluted area based on the online approach considering aqueous phase chemistry. In particular, the change in onset time and intensity of precipitation hours can have a severe and important impact on the regional daily meteorological fields, particularly over the Korean Peninsula. The results through complex aerosol-cloud-radiation interaction examined in this study over Northeast Asia can have profound and serious implications to the regional cloud and precipitation, and therefore immediate follow-up studies would be needed.

We also found out here some results with big discrepancies in comparison with the previous results, particularly regarding the aerosol indirect effects dominated only in unpolluted marine/coastal areas with low-cloud cover. Therefore, as a future study, multiple sensitivity experiments that apply more comprehensive aerosol treatments should be conducted against well-designed field studies considering various cloud and precipitation conditions over Northeast Asia. Those are to better understand the aerosol feedback mechanism in the online-coupled WRF-Chem model.

#### Acknowledgments

We thank National Institute of Environmental Research (NIER) for providing the MAPS-Seoul 2015 campaign measurements, and also thank KMA for providing meteorological observation data and computer resources. We also thank NOAA members for supporting to install WRF-Chem, and this research was partially supported by National Research Foundation of Korea funded by the Ministry of Education (NRF-2015R1D1A1A01060088).

#### Appendix A. Supplementary data

Supplementary data related to this article can be found at <http://dx.doi.org/10.1016/j.atmosenv.2017.10.044>.

#### References

- Abdul-Razzak, H., Ghan, S.J., 2000. A parameterization of aerosol activation 2. Multiple aerosol types. *J. Geophys. Res.* 105, 6837–6844. <http://dx.doi.org/10.1029/1999JD901161>.
- Abdul-Razzak, H., Ghan, S.J., 2002. A parameterization of aerosol activation 3. Sectional representation. *J. Geophys. Res.* 107, 4026. <http://dx.doi.org/10.1029/2001JD000483>.
- Albrecht, B.A., 1989. Aerosols, cloud microphysics, and fractional cloudiness. *Science* 245, 1227–1230.
- Archer-Nicholls, S., Lowe, D., Schultz, D.M., McFiggans, G., 2016. Aerosol-radiation-cloud interactions in a regional coupled model: the effects of convective parameterisation and resolution. *Atmos. Chem. Phys.* 16, 5573–5594.
- Barnard, J.C., Fast, J.D., Paredes-Miranda, G., Arnott, W.P., Laskin, A., 2010. Technical note: evaluation of the WRF-Chem “aerosol chemical to aerosol optical properties” module using data from the MILAGRO campaign. *Atmos. Chem. Phys.* 10, 7325–7340. <http://dx.doi.org/10.5194/acp-10-7325-2010>.
- Boltzmann, L., 1884. Ableitung des Stefan'schen Gesetzes, betreffend die Abhängigkeit der Wärmestrahlung von der Temperatur aus der elektromagnetischen Lichttheorie. *Ann. Phys. Chem. Ger.* 258 (6), 291–294. <http://dx.doi.org/10.1002/andp.18842580616>.
- Brunner, D., Savage, N., Jorba, O., Eder, B., Giordano, L., Badia, A., Balzarini, A., Baró, R., Bianconi, R., Chemel, C., Curci, G., Forkel, R., Jiménez-Guerrero, P., Hirtl, M., Hodzic, A., Honzak, L., Im, U., Knoté, C., Makar, P., Manders-Groot, A., van Meijgaard, E., Neal, L., Pérez, J.L., Pirovano, G., San Jose, R., Schröder, W., Sokhi, R.S., Syrakov, D., Torian, A., Tuccella, P., Werhahn, J., Wolke, R., Yahya, K., Zabkar, R., Zhang, Y., Hogrefe, C., Galmarini, S., 2015. Comparative analysis of meteorological performance of coupled chemistry-meteorology models in the context of AQMEII phase 2. *Atmos. Environ.* 115, 470–498.
- Canagaratna, M., Jayne, J., Jimenez, J., Allan, J., Alfarra, M., Zhang, Q., Onasch, T., Drewnick, F., Coe, H., Middlebrook, A., 2007. Chemical and microphysical characterization of ambient aerosols with the aerodyne aerosol mass spectrometer. *Mass Spectrom. Rev.* 26, 185–222.
- Carmichael, G.R., Calori, G., Hayami, H., Uno, I., Cho, S.Y., Engardt, M., Kim, S.B., Ichikawa, Y., Ikeda, Y., Woo, J.H., Ueda, H., Amann, M., 2002. The MICS-Asia study: model intercomparison of long-range transport and sulfur deposition in East Asia. *Atmos. Environ.* 36, 175–199.
- Chapman, E.G., Gustafson Jr., W.I., Easter, R.C., Barnard, J.C., Ghan, S.J., Pekour, M.S., Fast, J.D., 2009. Coupling aerosol-cloud-radiative processes in the WRF-Chem model: investigating the radiative impact of elevated point sources. *Atmos. Chem. Phys.* 9, 945–964. <http://dx.doi.org/10.5194/acp-9-945-2009>.
- Cheng, W.Y.Y., Steenburgh, W.J., 2005. Evaluation of surface sensible weather forecasts by the WRF and the Eta models over the western United States. *Wea. Forecast* 20, 812–821.
- DeCarlo, P.F., Kimmel, J.R., Trimborn, A., Northway, M.J., Jayne, J.T., Aiken, A.C., Gonin, M., Fuhrer, K., Horvath, T., Docherty, K.S., 2006. Field-deployable, high-resolution, time-of-flight aerosol mass spectrometer. *Anal. Chem.* 78, 8281–8289.
- Drewnick, F., Hings, S.S., DeCarlo, P., Jayne, J.T., Gonin, M., Fuhrer, K., Weimer, S., Jimenez, J.L., Demerjian, K.L., Borrmann, S., 2005. A new time-of-flight aerosol mass spectrometer (TOF-AMS) - instrument description and first field deployment. *Aerosol Sci. Tech.* 39, 637–658.
- Easter, R.C., Ghan, S.J., Zhang, Y., Saylor, R.D., Chapman, E.G., Laulainen, N.S., Abdul-Razzak, H., Leung, L.R., Bian, X., Zaveri, R.A., 2004. MIRAGE: model description and evaluation of aerosols and trace gases. *J. Geophys. Res.* 109, D20210. <http://dx.doi.org/10.1029/2004JD004571>.
- Emmons, L.K., Walters, S., Hess, P.G., Lamarque, J.-F., Pfister, G.G., Fillmore, D., Granier, C., Guenther, A., Kinnison, D., Laepple, T., Orlando, J., Tie, X., Tyndall, G., Wiedinmyer, C., Baugheun, S.L., Kloster, S., 2010. Description and evaluation of the model for ozone and related chemical Tracers, version 4 (MOZART-4). *Geosci. Model Dev.* 3, 43–67. <http://dx.doi.org/10.5194/gmd-3-43-2010>.
- Fan, J., Leung, L.R., Li, Z., Morrison, H., Chen, H., Zhou, Y., Qian, Y., Wang, Y., 2012. Aerosol impacts on clouds and precipitation in eastern China: results from bin and bulk microphysics. *J. Geophys. Res.* 117, D00K36. <http://dx.doi.org/10.1029/2011JD016537>.
- Fast, J.D., Gustafson Jr., W.I., Easter, R.C., Zaveri, R.A., Barnard, J.C., Chapman, E.G.,

- Grell, G.A., Peckham, S.E., 2006. Evolution of ozone, particulates, and aerosol direct radiative forcing in the vicinity of Houston using a fully coupled meteorology-chemistry-aerosol model. *J. Geophys. Res.* 111, D21305. <http://dx.doi.org/10.1029/2005JD006721>.
- Forkel, R., Balzarini, A., Baró, R., Bianconi, R., Curci, G., Jiménez-Guerrero, P., Hirtl, M., Honzak, L., Lorenz, C., Im, U., Pérez, J.L., Pirovano, G., San José, R., Tuccella, P., Werhahn, J., Žabkar, R., 2015. Analysis of the WRF-Chem contributions to AQMEII phase2 with respect to aerosol radiative feedbacks on meteorology and pollutant distributions. *Atmos. Environ.* 115, 630–645.
- Forkel, R., Werhahn, J., Hansen, A.B., McKeen, S., Peckham, S., Grell, G., Suppan, P., 2012. Effect of aerosol-radiation feedback on regional air quality - a case study with WRF/Chem. *Atmos. Environ.* 53, 202–211.
- Gao, M., Liu, Z., Wang, Y., Lu, X., Ji, D., Wang, L., Li, M., Wang, Z., Zhang, Q., Carmichael, G.R., 2017. Distinguishing the roles of meteorology, emission control measures, regional transport, and co-benefits of reduced aerosol feedbacks in “APEC Blue”. *Atmos. Environ.* <http://dx.doi.org/10.1016/j.atmosenv.2017.08.054>.
- Gao, Y., Zhang, M., Liu, Z., Wang, L., Wang, P., Xia, X., Tao, M., Zhu, L., 2015. Modeling the feedback between aerosol and meteorological variables in the atmospheric boundary layer during a severe fog-haze event over the North China Plain. *Atmos. Chem. Phys.* 15, 4279–4295.
- Ghan, S., Laulainen, N., Easter, R., Wagener, R., Nemesure, S., Chapman, E., Zhang, Y., Leung, R., 2001. Evaluation of aerosol direct radiative forcing in MIRAGE. *J. Geophys. Res.* 106, 5295–5316.
- Grell, G.A., Peckham, S.E., Schmitz, R., McKeen, S.A., Frost, G., Skamarock, W.C., Eder, B., 2005. Fully coupled “online” chemistry within the WRF model. *Atmos. Environ.* 39, 6957–6975.
- Grosvenor, D.P., Field, P.R., Hill, A.A., Shipway, B.J., 2017. The relative importance of macrophysical and cloud albedo changes for aerosol-induced radiative effects in closed-cell stratocumulus: insight from the modelling of a case study. *Atmos. Chem. Phys.* 17, 5155–5183. <http://dx.doi.org/10.5194/acp-17-5155-2017>.
- Guenther, A., Karl, T., Harley, P., Wiedinmyer, C., Palmer, P.I., Geron, C., 2006. Estimates of global terrestrial isoprene emissions using MEGAN (model of emissions of gases and aerosols from nature). *Atmos. Chem. Phys.* 6, 3181–3210. <http://dx.doi.org/10.5194/acp-6-3181-2006>.
- Gustafson Jr., W.I., Chapman, E.G., Ghan, S.J., Easter, R.C., Fast, J.D., 2007. Impact on modeled cloud characteristics due to simplified treatment of uniform cloud condensation nuclei during NEAQS 2004. *Geophys. Res. Lett.* 34, L19809. <http://dx.doi.org/10.1029/2007GL030021>.
- Harris, E., Sinha, B., van Pinxteren, D., Tilgner, A., Fomba, K.W., Schneider, J., Roth, A., Gnauk, T., Fahlbusch, B., Mertes, S., Lee, T., Collett, J., Foley, S., Borrmann, S., Hoppe, P., Herrmann, H., 2013. Enhanced role of transition metal ion catalysis during in-cloud oxidation of SO<sub>2</sub>. *Science* 340, 727–730.
- Haywood, J., Boucher, O., 2000. Estimates of the direct and indirect radiative forcing due to tropospheric aerosols: a review. *Rev. Geophys.* 38, 513–543.
- Hong, C., Zhang, Q., Zhang, Y., Tang, Y., Tong, D., He, K., 2017. Multi-year downscaling application of two-way coupled WRF v3.4 and CMAQ v5.0.2 over east Asia for regional climate and air quality modeling: model evaluation and aerosol direct effects. *Geosci. Model Dev.* 10, 2447–2470.
- Huffman, G.J., Adler, R.F., Bolvin, D.T., Gu, G., Nelkin, E.J., Bowman, K.P., Hong, Y., Stocker, E.F., Wolff, D.B., 2007. The TRMM multisatellite precipitation analysis (TMPA): quasi-global, multiyear, Combined-sensor precipitation estimates at fine scales. *J. Hydrometeorol.* 8 (1), 38–55.
- Jayne, J.T., Leard, D.C., Zhang, X., Davidovits, P., Smith, K.A., Kolb, C.E., Worsnop, D.R., 2000. Development of an aerosol mass spectrometer for size and composition analysis of submicron particles. *Aerosol Sci. Tech.* 33, 49–70.
- Jiang, F., Liu, Q., Huang, X., Wang, T., Zhuang, B., Xie, M., 2012. Regional modeling of secondary organic aerosol over China using WRF/Chem. *J. Aerosol Sci.* 43, 57–73.
- Jimenez, J.L., Jayne, J.T., Shi, Q., Kolb, C.E., Worsnop, D.R., Yourshaw, I., Seinfeld, J.H., Flagan, R.C., Zhang, X., Smith, K.A., Morris, J.W., Davidovits, P., 2003. Ambient aerosol sampling using the aerodyne aerosol mass spectrometer. *J. Geophys. Res.* 108 (D7). <http://dx.doi.org/10.1029/2001JD001213>.
- Kim, B.-G., Schwartz, S.E., Miller, M.A., Min, Q., 2003. Effective radius of cloud droplets by ground-based remote sensing: relationship to aerosol. *J. Geophys. Res.* 108 (D23). <http://dx.doi.org/10.1029/2003JD003721>.
- Kim, C.-H., Park, S.-Y., Kim, Y.-J., Chang, L.-S., Song, S.-K., Moon, Y.-S., Song, C.-K., 2012. A numerical study on indicators of long-range transport potential for anthropogenic particulate matters over northeast Asia. *Atmos. Environ.* 58, 35–44.
- Kim, B.-U., Bae, C., Kim, H.C., Kim, E., Kim, S., 2017a. Spatially and chemically resolved source apportionment analysis: case study of high particulate matter event. *Atmos. Environ.* 162, 55–70.
- Kim, N., Park, M., Yum, S.S., Park, J.S., Song, I.H., Shin, H.J., Ahn, J.Y., Kwak, K.-H., Kim, H., Bae, G.-N., Lee, G., 2017b. Hygroscopic properties of urban aerosols and their cloud condensation nuclei activities measured in Seoul during the MAPS-Seoul campaign. *Atmos. Environ.* 153, 217–232.
- Kong, X., Forkel, R., Sokhi, R.S., Suppan, P., Baklanov, A., Gauss, M., Brunner, D., Baró, R., Balzarini, A., Chemel, C., Curci, G., Jiménez-Guerrero, P., Hirtl, M., Honzak, L., Im, U., Pérez, J.L., Pirovano, G., San José, R., Schlüzen, K.H., Tsegas, G., Tuccella, P., Werhahn, J., Žabkar, R., Galmarini, S., 2015. Analysis of meteorology-chemistry interactions during air pollution episodes using online coupled models within AQMEII phase-2. *Atmos. Environ.* 115, 527–540.
- Kourtidis, K., Stathopoulos, S., Georgoulas, A.K., Alexandri, G., Rapsomanikis, S., 2015. A study of the impact of synoptic weather conditions and water vapor on aerosol-cloud relationships over major urban clusters of China. *Atmos. Chem. Phys.* 15, 10955–10964.
- Lee, H.-J., Kim, C.-H., 2016. Transport/transformations study during the MAPS (pre-KORUS-AQ) field campaign. In: 17th Annual WRF Users' Workshop. NCAR, Boulder, CO, USA.
- Lee, T., Choi, J., Lee, G., Ahn, J., Park, J.S., Atwood, S.A., Schurman, M., Choi, Y., Chung, Y., Collett Jr., J.L., 2015. Characterization of aerosol composition, concentrations, and sources at Baengnyeong Island, Korea using an aerosol mass spectrometer. *Atmos. Environ.* 120, 297–306.
- Li, M., Zhang, Q., Streets, D.G., He, K.B., Cheng, Y.F., Emmons, L.K., Huo, H., Kang, S.C., Lu, Z., Shao, M., Su, H., Yu, X., Zhang, Y., 2014. Mapping Asian anthropogenic emissions of non-methane volatile organic compounds to multiple chemical mechanisms. *Atmos. Chem. Phys.* 14, 5617–5638.
- Li, M., Zhang, Q., Kurokawa, J., Woo, J.-H., He, K., Lu, Z., Ohara, T., Song, Y., Streets, D.G., Carmichael, G.R., Cheng, Y., Hong, C., Huo, H., Jiang, X., Kang, S., Liu, F., Su, H., Zheng, B., 2017. MIX: a mosaic Asian anthropogenic emission inventory under the international collaboration framework of the MICS-Asia and HTAP. *Atmos. Chem. Phys.* 17, 935–963.
- Li, Y., Daum, P.H., McGraw, R.L., 2005. Size truncation effect, threshold behavior, and a new type of autoconversion parameterization. *Geophys. Res. Lett.* 32, L11811. <http://dx.doi.org/10.1029/2005GL022636>.
- Mashayekhi, R., Sloan, J.J., 2014. Effects of aerosols on precipitation in north-eastern North America. *Atmos. Chem. Phys.* 14, 5111–5125.
- Matsui, H., Koike, M., Kondo, Y., Takegawa, N., Kita, K., Miyazaki, Y., Hu, M., Chang, S.Y., Blake, D.R., Fast, J.D., Zaveri, R.A., Streets, D.G., Zhang, Q., Zhu, T., 2009. Spatial and temporal variations of aerosols around Beijing in summer 2006: model evaluation and source apportionment. *J. Geophys. Res.* 114, D00G13. <http://dx.doi.org/10.1029/2008jd010906>.
- Molders, N., Tran, H.N.Q., Cahill, C.F., Leelasakultum, K., Tran, T.T., 2012. Assessment of WRF/Chem PM2.5 forecasts using mobile and fixed location data from the Fairbanks, Alaska winter 2008/09 field campaign. *Atmos. Pollut. Res.* 3, 180–191.
- NCEP, 2000. NCEP FNL Operational Model Global Tropospheric Analyses, Continuing from July 1999. <http://dx.doi.org/10.5065/D6M043C6>.
- Ohara, T., Akimoto, H., Kurokawa, J., Horii, N., Yamaji, K., Yan, X., Hayasaka, T., 2007. *Atmos. Chem. Phys.* 7, 4419–4444.
- Park, I.-S., Choi, W.-J., Lee, T.-Y., Lee, S.-J., Han, J.-S., Kim, C.-H., 2005. Simulation of long-range transport of air pollutants over Northeast Asia using a comprehensive acid deposition model. *Atmos. Environ.* 39, 4075–4085.
- Peckham, S., Grell, G.A., McKeen, S.A., Barth, M., Pfister, G., Wiedinmyer, C., Fast, J.D., Gustafson, W.I., Zaveri, R., Easter, R.C., Barnard, J., Chapman, E., Hewson, M., Schmitz, R., Salzmann, M., Freitas, S., 2011. WRF/Chem Version 3.3 User's Guide. NOAA Technical Memo. 98 pp.
- Piccot, S.D., Watson, J.J., Jones, J.W., 1992. Global inventory of volatile organic compound emissions from anthropogenic sources. *J. Geophys. Res.* 97, 9897–9912.
- Pincus, R., Baker, M.B., 1994. Effect of precipitation on the albedo susceptibility of clouds in the marine boundary layer. *Nature* 372, 250–252. <http://dx.doi.org/10.1038/372250a0>.
- Rieger, D., Bangert, M., Kottmeier, C., Vogel, H., Vogel, B., 2014. Impact of aerosol on post-frontal convective clouds over Germany. *Tellus B* 66, 22528. <http://dx.doi.org/10.3402/tellusb.v66.22528>.
- Rosenfeld, D., 2000. Suppression of rain and snow by urban and industrial air pollution. *Science* 287 (5459), 1793–1796.
- Rosenfeld, D., Lohmann, U., Raga, G.B., O'Dowd, C.D., Kulmala, M., Fuzzi, S., Reissell, A., Andreae, M.O., 2008. Flood or drought: how do aerosols affect precipitation? *Science* 321, 1309–1313.
- Rosenfeld, D., Sherwood, S., Wood, R., Donner, L., 2014. Climate effects of aerosol-cloud interactions. *Science* 343, 370–380.
- Saide, P.E., Spak, S.N., Carmichael, G.R., Mena-Carrasco, M.A., Yang, Q., Howell, S., Leon, D.C., Snider, J.R., Bandy, A.R., Collett, J.L., Benedict, K.B., de Szeoek, S.P., Hawkins, L.N., Allen, G., Crawford, I., Crosier, J., Springston, S.R., 2012. Evaluating WRF-Chem aerosol indirect effects in Southeast Pacific marine stratocumulus during VOCALS-REx. *Atmos. Chem. Phys.* 12, 3045–3064. <http://dx.doi.org/10.5194/acp-12-3045-2012>.
- Saikawa, E., Naik, V., Horowitz, L.W., Liu, J.F., Mauzerall, D.L., 2009. Present and potential future contributions of sulfate, black and organic carbon aerosols from China to global air quality, premature mortality and radiative forcing. *Atmos. Environ.* 43, 2814–2822.
- Skamarock, W.C., Klemp, J.B., Dudhia, J., Gill, D.O., Barker, D.M., Duda, M., Huang, X.-Y., Wang, W., Powers, J.G., 2008. A Description of the Advanced Research WRF Version 3. Technical Note 475+STR. NCAR, Boulder, CO, USA 113pp.
- Song, H., Wang, K., Zhang, Y., Hong, C., Zhou, S., 2017. Simulation and evaluation of dust emissions with WRF-Chem (v3.7.1) and its relationship to the changing climate over East Asia from 1980 to 2015. *Atmos. Environ.* <http://dx.doi.org/10.1016/j.atmosenv.2017.08.051>.
- Stefan, J., 1879. *Sitzungsberichte der mathematisch-naturwissenschaftlichen Classe der kaiserlichen Akademie der Wissenschaften (in German)* Vienna. Über die Beziehung zwischen der Wärmestrahlung und der Temperatur, vol. 79. pp. 391–428.
- Tao, Z., Yu, H., Chin, M., 2015. The role of aerosol-cloud-radiation interactions in regional air quality—a NU-WRF Study over the United States. *Atmosphere* 6, 1045–1068. <http://dx.doi.org/10.3390/atmos6081045>.
- Tuccella, P., Curci, G., Visconti, G., Bessagnet, B., Menut, L., Park, R.J., 2012. Modeling of gas and aerosol with WRF/Chem over Europe: evaluation and sensitivity study. *J. Geophys. Res.* 117, D03303. <http://dx.doi.org/10.1029/2011jd016302>.
- Twomey, S., 1977. The influence of pollution on the shortwave albedo of clouds. *J. Atmos. Sci.* 34, 1149–1152.
- Wang, F., Guo, J., Wu, Y., Zhang, X., Deng, M., Li, X., Zhang, J., Zhao, J., 2014. Satellite observed aerosol-induced variability in warm cloud properties under different meteorological conditions over eastern China. *Atmos. Environ.* 84, 122–132.
- Wang, F., Guo, J., Zhang, J., Huang, J., Min, M., Chen, T., Liu, H., Deng, M., Li, X., 2015a. Multi-sensor quantification of aerosol-induced variability in warm clouds over

- eastern China. *Atmos. Environ.* 113, 1–9.
- Wang, J., Xu, J., He, Y., Chen, Y., Meng, F., 2016. Long range transport of nitrate in the low atmosphere over Northeast Asia. *Atmos. Environ.* 144, 315–324.
- Wang, K., Zhang, Y., Yahya, K., Wu, S.-Y., Grell, G., 2015b. Implementation and initial application of new chemistry-aerosol options in WRF/Chem for simulating secondary organic aerosols and aerosol indirect effects for regional air quality. *Atmos. Environ.* 115, 716–732.
- Woo, J.-H., Quan, S., Choi, K.-C., Kim, H., Jin, H., Song, C.-K., Han, J., Lee, S., 2014. Development of the comprehensive regional emissions inventory for atmospheric transport experiment (CREATE) inventory in support of integrated modeling of climate and air quality for east Asia. In: 16th GEIA Conference. NCAR, Boulder, CO, USA.
- Wu, J., Li, G., Cao, J., Bei, N., Wang, Y., Feng, T., Huang, R., Liu, S., Zhang, Q., Tie, X., 2017. Contributions of trans-boundary transport to summertime air quality in Beijing, China. *Atmos. Chem. Phys.* 17, 2035–2051. <http://dx.doi.org/10.5194/acp-17-2035-2017>.
- Yahya, K., Wang, K., Gudoshava, M., Glotfelty, T., Zhang, Y., 2015. Application of WRF/Chem over North America under the AQMEII phase 2: Part I. Comprehensive evaluation of 2006 simulation. *Atmos. Environ.* 115, 733–755.
- Yang, Q., Gustafson Jr., W.I., Fast, J.D., Wang, H., Easter, R.C., Morrison, H., Lee, Y.-N., Chapman, E.G., Spak, S.N., Mena-Carrasco, M.A., 2011. Assessing regional scale predictions of aerosols, marine stratocumulus, and their interactions during VOCALS-REx using WRF-Chem. *Atmos. Chem. Phys.* 11, 11951–11975. <http://dx.doi.org/10.5194/acp-11-11951-2011>.
- Zhang, B., Wang, Y., Hao, J., 2015. Simulating aerosol-radiation-cloud feedbacks on meteorology and air quality over eastern China under severe haze conditions in winter. *Atmos. Chem. Phys.* 15, 2387–2404.
- Zhang, Y., Wen, X.-Y., Jang, C., 2010. Simulating chemistry-aerosol-cloud-radiation-climate feedbacks over the continental US using the online-coupled Weather Research Forecasting Model with chemistry (WRF/Chem). *Atmos. Environ.* 44, 3568–3582.
- Zhao, Z., Pritchard, M.S., Russell, L.M., 2012. Effects on precipitation, clouds, and temperature from long-range transport of idealized aerosol plumes in WRF-Chem simulations. *J. Geophys. Res.* 117, D05206. <http://dx.doi.org/10.1029/2011JD016744>.
- Zhou, C., Zhang, X., Gong, S., Wang, Y., Xue, M., 2016. Improving aerosol interaction with clouds and precipitation in a regional chemical weather modeling system. *Atmos. Chem. Phys.* 16, 145–160.